Kinetic multi-layer model of gas-particle interactions in aerosols and clouds (KM-GAP): linking condensation, evaporation and chemical reactions of organics, oxidants and water

Atmos. Chem. Phys. Discuss., 11, 33689–33732, 2011
www.atmos-chem-phys-discuss.net/11/33689/2011/
doi:10.5194/acpd-11-33689-2011

Atmospheric Chemistry and Physics Discussions

Kinetic multi-layer model of gas-particle interactions in aerosols and clouds (KM-GAP): linking condensation, evaporation and chemical reactions of organics, oxidants and water

M. Shiraiwa[1], C. Pfrang[2], T. Koop[3], and U. Pöschl[1]

[1]Max Planck Institute for Chemistry, Biogeochemistry Department, P.O. Box 3060, 55128 Mainz, Germany
[2]University of Reading, Department of Chemistry, P.O. Box 224, Whiteknights, Reading RG6 6AD, UK
[3]Bielefeld University, Faculty of Chemistry, Universitätsstraße 25, 33615, Bielefeld, Germany

Received: 14 December 2011 – Accepted: 15 December 2011 – Published: 21 December 2011

Correspondence to: M. Shiraiwa (m.shiraiwa@mpic.de)

Published by Copernicus Publications on behalf of the European Geosciences Union.

Abstract

We present a novel kinetic multi-layer model for gas-particle interactions in aerosols and clouds (KM-GAP) that treats explicitly all steps of mass transport and chemical reaction of semi-volatile species partitioning between gas phase, particle surface and particle bulk. KM-GAP is based on the PRA model framework (Pöschl-Rudich-Ammann, 2007), and it includes gas phase diffusion, reversible adsorption, surface reactions, bulk diffusion and reaction, as well as condensation, evaporation and heat transfer. The size change of atmospheric particles and the temporal evolution and spatial profile of the concentration of individual chemical species can be modeled along with gas uptake and accommodation coefficients. Depending on the complexity of the investigated system, unlimited numbers of semi-volatile species, chemical reactions, and physical processes can be treated, and the model shall help to bridge gaps in the understanding and quantification of multiphase chemistry and microphysics in atmospheric aerosols and clouds.

In this study we demonstrate how KM-GAP can be used to analyze, interpret and design experimental investigations of changes in particle size and chemical composition in response to condensation, evaporation, and chemical reaction. For the condensational growth of water droplets, our kinetic model results provide a direct link between laboratory observations and molecular dynamic simulations, confirming that the accommodation coefficient of water at ~270 K is close to unity. Literature data on the evaporation of dioctyl phthalate as a function of particle size and time can be reproduced, and the model results suggest that changes in the experimental conditions like aerosol particle concentration and chamber geometry may influence the evaporation kinetics and can be optimized for efficient probing of specific physical effects and parameters. With regard to oxidative aging of organic aerosol particles, we illustrate how the formation and evaporation of volatile reaction products like nonanal can cause a decrease in the size of oleic acid particles exposed to ozone.

1 Introduction

Aerosol particles are ubiquitous in the atmosphere and play a critical role in global climate, air quality, atmospheric chemistry and public health (Andreae and Crutzen, 1997; Pöschl, 2005). The interactions of atmospheric particles with water vapor can lead to the formation of cloud droplets or ice crystals depending on size, phase state and hygroscopicity, influencing radiative budget and precipitation (Koop et al., 2000; Andreae and Rosenfeld, 2008; Murray et al., 2010; Pöschl et al., 2010). The interactions of aerosol particles with atmospheric oxidants can affect the abundance of trace gases and significantly alter physical and chemical properties of aerosols such as toxicity, reactivity, ice and cloud condensation nucleation abilities, and radiative properties (Finlayson-Pitts and Pitts, 1997; George and Abbatt, 2010b; Kolb et al., 2010; Kuwata et al., 2011; Lu et al., 2011; Schwier et al., 2011; Shiraiwa et al., 2011b; Wang and Knopf, 2011). Gas-particle partitioning of semi-volatile species is a key process for formation and aging of secondary organic aerosol (Odum et al., 1996; Seinfeld and Pankow, 2003; Donahue et al., 2006; Robinson et al., 2007; Hallquist et al., 2009; Jimenez et al., 2009; Riipinen et al., 2011).

Atmospheric particles consist of a wide variety of organic and inorganic chemical compounds which can occur as different phase states of liquid, semi-solid or solid states (crystalline, amorphous, glassy, ultraviscous, gel-like) depending on their composition and ambient conditions (Marcolli et al., 2004; Zobrist et al., 2008; Mikhailov et al., 2009; Virtanen et al., 2010; Koop et al., 2011). The phase state can influence the gas-particle partitioning and heterogeneous reactions and multiphase processes in atmospheric aerosols (Knopf et al., 2005; Nash et al., 2006; Renbaum and Smith, 2009; Cappa and Wilson, 2011; Pfrang et al., 2011; Shiraiwa et al., 2011a; Vaden et al., 2011). Chemical reactions can proceed in both gas and condensed phase but it is often difficult to discriminate gas, surface and bulk reactions. Moreover, the relative importance of them for secondary organic aerosol formation and aging is poorly understood (Moise and Rudich, 2000; Kalberer et al., 2004; McNeill et al., 2008; Hallquist et

al., 2009; George and Abbatt, 2010a; Fry et al., 2011; Loza et al., 2011; Salo et al., 2011). So far resistor model formulations are widely used to describe and investigate heterogeneous reactions and multiphase processes in laboratory, field and model studies of atmospheric chemistry (Hanson, 1997; Finlayson-Pitts and Pitts, 2000; Worsnop et al., 2002; Anttila et al., 2006; King et al., 2009; Xiao and Bertram, 2011). The traditional resistor models, however, are usually based on simplifying assumptions such as steady state conditions, homogeneous mixing, and limited numbers of non-interacting species and processes.

In order to overcome these limitations, Pöschl, Rudich and Ammann (Pöschl et al., 2007) have developed a kinetic model framework (PRA framework) with a double-layer surface concept and universally applicable rate equations and parameters for mass transport and chemical reactions at the gas-particle interface of aerosols and clouds. Ammann and Pöschl (2007) provided first examples on how the PRA framework can be applied to describe various physico-chemical processes in aerosols and clouds such as reactive gas uptake on solid particles and solubility saturation of liquid droplets under transient or steady-state conditions. Shiraiwa et al. (2009) presented a kinetic double-layer surface model (K2-SURF) for the degradation of a wide range of polycyclic aromatic hydrocarbons (PAHs) by multiple photo-oxidants (O_3, NO_2, OH and NO_3). Using K2-SURF Shiraiwa et al. (2011b) showed that a long-lived reactive oxygen intermediate is formed in the reaction of ozone with aerosol particles. Springmann et al. (2009) and Kaiser et al. (2011) demonstrated the applicability and usefulness of the PRA framework in an urban plume box model of the degradation of benzo[a]pyrene on soot by ozone and nitrogen dioxide. Pfrang et al. (2010) developed a kinetic double-layer model coupling aerosol surface and bulk chemistry (K2-SUB), in which mass transport and chemical reactions in the bulk are not explicitly resolved but represented by a reacto-diffusive flux. Shiraiwa et al. (2010) developed a kinetic multi-layer model of aerosol surface and bulk chemistry (KM-SUB) that explicitly treats all steps of mass transport and chemical reaction from the gas-particle interface to the particle core, resolving concentration gradients and diffusion throughout the particle bulk. Pfrang et

al. (2011) applied and extended KM-SUB to investigate the impact of transformation of diffusivity on the chemical aging of multi-component organic aerosol particles.

Here we present a kinetic multi-layer model of gas-particle interactions in aerosols and clouds (KM-GAP) that builds on KM-SUB and explicitly treats all steps of mass transport and chemical reaction from the gas phase to the particle core, including the evaporation and condensation of semi-volatile species. We demonstrate the applicability of KM-GAP for the condensation of water and the oxidation and evaporation of organics. The model results are compared with earlier experimental and theoretical studies.

2 Model description

As illustrated in Fig. 1, KM-GAP consists of multiple model compartments and layers, respectively: gas phase, near-surface gas phase, sorption layer, quasi-static surface layer, and near-surface bulk. The sorption and quasi-static surface layer has a monolayer thickness that corresponds to the (average) effective molecular diameter of semi-volatile species Z_i (δ_{Z_i}). The following processes are considered in KM-GAP: gas phase diffusion, gas-surface transport (reversible adsorption), surface-bulk transport, surface and bulk reactions, bulk diffusion, vapor pressure change, and heat transfer. The following differential equations can be used to describe the mass balance of each molecule Z_i for surface and each bulk layers:

$$\mathrm{d}N_{Z_i,\mathrm{s}}/\mathrm{d}t = (J_{\mathrm{ads},Z_i} - J_{\mathrm{des},Z_i} + P_{\mathrm{s},Z_i} - L_{\mathrm{s},Z_i} - J_{\mathrm{s,ss},Z_i} + J_{\mathrm{ss,s},Z_i})\ A_{\mathrm{ss}} \quad (1)$$

$$\mathrm{d}N_{Z_i,\mathrm{ss}}/\mathrm{d}t = (J_{\mathrm{s,ss},Z_i} - J_{\mathrm{ss,s},Z_i} + P_{\mathrm{ss},Z_i} - L_{\mathrm{ss},Z_i} - J_{\mathrm{ss,b1},Z_i} + J_{\mathrm{b1,ss},Z_i})\ A(1) \quad (2)$$

$$\mathrm{d}N_{Z_i,\mathrm{b1}}/\mathrm{d}t = (J_{\mathrm{ss,b1},Z_i} - J_{\mathrm{b1,ss},Z_i})\ A(1) + (J_{\mathrm{b1,b2},Z_i} - J_{\mathrm{b2,b1},Z_i})\ A(2) + (P_{\mathrm{b1},Z_i} - L_{\mathrm{b1},Z_i})V(1) \quad (3)$$

$$\mathrm{d}N_{Z_i,\mathrm{b}k}/\mathrm{d}t = (J_{\mathrm{b}k-1,\mathrm{b}k,Z_i} - J_{\mathrm{b}k,\mathrm{b}k-1,Z_i})\ A(k) + (J_{\mathrm{b}k+1,\mathrm{b}k,Z_i} - J_{\mathrm{b}k,\mathrm{b}k+1,Z_i})\ A(k+1) + (P_{\mathrm{b}k,Z_i} - L_{\mathrm{b}k,Z_i})\ V(k) \quad (k = 2,\ldots,n-1) \quad (4)$$

$$\mathrm{d}N_{Z_i,\mathrm{b}n}/\mathrm{d}t = (J_{\mathrm{b}n-1,\mathrm{b}n,Z_i} - J_{\mathrm{b}n,\mathrm{b}n-1,Z_i})\ A(n) + (P_{\mathrm{b}n,Z_i} - L_{\mathrm{b}n,Z_i})\ V(n) \quad (5)$$

where $N_{Z_i,\mathrm{s}}$, $N_{Z_i,\mathrm{ss}}$, and $N_{Z_i,\mathrm{b}k}$ are the absolute number of Z_i molecules at surface, at quasi-static surface layer, and at bulk layer k, respectively The various types of mass transport fluxes (J) and rates of chemical production and loss (P, L) are defined in the list of symbols (Table A1). $A(k)$ and $V(k)$ are the outer surface area and the volume of the bulk layer k, respectively (Fig. 1). The volume of each layer $V(k)$ can be calculated using $N_{Z_i,\mathrm{b}k}$ and molecular volume V_{Z_i} assuming ideal mixing (volume additivity)

$$V(k) = \sum_i N_{Z_i,\mathrm{b}k} V_{Z_i} \quad (6)$$

For spherical particles, the radius position $r(k)$, the outer surface area $A(k)$ and the layer thickness $\delta(k)$ of the bulk layer k and particle diameter d_{p} can be calculated as follows:

$$r(k) = \left[\frac{3}{4\pi}\sum_{j=k}^{n} V(j)\right]^{1/3} \quad (7)$$

$$A(k) = 4\pi r(k)^2 \quad (8)$$

$$\delta(k) = r(k) - r(k-1) \quad (9)$$

$$d_{\mathrm{p}} = 2r_{\mathrm{p}} = 2(r(1) + \delta_{Z_i}) \quad (10)$$

In this way, each layer can either shrink or grow, in response to mass transport and chemical reactions. KM-GAP can also deal with planar geometry (thin films) assuming $A(k)$ is constant.

The surface and bulk number concentrations of Z_i can be calculated as follows:

$$[Z_i]_{\mathrm{s}} = N_{Z_i,\mathrm{s}}/A_{\mathrm{ss}} \quad (11)$$

$$[Z_i]_{ss} = N_{Z_i,ss}/A(1) \quad (12)$$

$$[Z_i]_{bk} = N_{Z_i,bk}/V(k) \quad (13)$$

The uptake coefficient of gas species Z_i can be expressed as a ratio between the net fluxes of Z_i from the gas phase to the condensed phase J_{net,Z_i}, and the collision flux J_{coll,Z_i}.

$$\gamma_{Z_i} = \frac{J_{net,Z_i}}{J_{coll,Z_i}} = \frac{J_{ads,Z_i} - J_{des,Z_i}}{J_{coll,Z_i}} \quad (14)$$

Note that γ_{Z_i} is $0 \le \gamma_{Z_i} \le 1$ when Z_i is adsorbing/condensing onto a surface (particle growth), whereas γ_{Z_i} can be negative when Z_i is desorbing/evaporating from a surface (particle shrink). The change of gas phase concentration of Z_i can be described using J_{net,Z_i} as follows:

$$\frac{d[Z_i]_g}{dt} = -\sum_{m}^{N_p} J_{net,Z_i} A_{ss,m} \quad (15)$$

where N_p is the number concentration of aerosol particles and $A_{ss,m}$ is the surface area of the particle m. In case of monodispersed particles the above equation is reduced to:

$$\frac{d[Z_i]_g}{dt} = -N_p J_{net,Z_i} A_{ss} \quad (16)$$

In the following sub-sections we specify the formalisms used to describe and calculate fluxes or rates of gas-surface interactions, surface reaction, surface-bulk transport, bulk diffusion and bulk reactions.

Note that KM-GAP can treat species of any volatility, without the need to constrain any species to just one phase (aerosol or gas), i.e. it effectively treats each species Z_i as semi-volatile. In the kinetic models previously developed by the authors, the volatile

species X and non-volatile species Y were treated separately (Shiraiwa et al., 2009, 2010; Pfrang et al., 2010), but the distinction between them is removed now in the KM-GAP model presented here.

2.1 Interfacial transport and surface reactions

Based on kinetic theory, the gas kinetic flux of Z_i colliding with the surface J_{coll,Z_i} can be expressed as

$$J_{coll,Z_i} = [Z_i]_{gs}\omega_{Z_i}/4 \quad (17)$$

where $[Z_i]_{gs}$ is near-surface gas phase concentration of Z_i and ω_{Z_i} is mean thermal velocity given by $\omega_{Z_i} = (8RT/(\pi M_{Z_i}))^{1/2}$, where M_{Z_i} is the molar mass of Z_i, R is the gas constant, and T is the absolute temperature. The significant net uptake of Z_i will lead to local depletion of concentration at near-surface gas phase ($[Z_i]_{gs} < [Z_i]_g$) and gas phase diffusion will influence further uptake. In this case near-surface gas phase concentration should be corrected using a gas phase diffusion correction factor C_{g,Z_i}.

$$[Z_i]_{gs} = C_{g,Z_i}[Z_i]_g \quad (18)$$

C_{g,Z_i} can be described as follows (Pöschl et al., 2007).

$$C_{g,Z_i} = \frac{1}{1 + \gamma_{Z_i}\frac{0.75+0.28Kn_{Z_i}}{Kn_{Z_i}(1+Kn_{Z_i})}} \quad (19)$$

γ_{Z_i} is the uptake coefficients of Z_i, which can be calculated as described below in Eq. (18). Kn_{Z_i} is the Knudsen number which can be approximated by the gas phase diffusion coefficient D_{g,Z_i} and particle diameter d_p.

$$Kn_{Z_i} = \frac{6D_{g,Z_i}}{\omega_{Z_i} d_p} \quad (20)$$

The flux of adsorption of gas molecules on the quasi-static particle surface can be expressed as

$$J_{\mathrm{ads},\mathrm{Z}_i} = \alpha_{\mathrm{s},\mathrm{Z}_i} J_{\mathrm{coll},\mathrm{Z}_i} = k_{\mathrm{a},\mathrm{Z}_i}[\mathrm{Z}_i]_{\mathrm{g}} \quad (21)$$

where $\alpha_{\mathrm{s},\mathrm{Z}_i}$ is surface accommodation coefficient and $k_{\mathrm{a},\mathrm{Z}_i}$ ($=\alpha_{\mathrm{s},\mathrm{Z}_i}\omega_{\mathrm{Z}_i}/4$) is a first-order adsorption rate coefficient. $\alpha_{\mathrm{s},\mathrm{Z}_i}$ is determined by the surface accommodation coefficient on an adsorbate-free surface $\alpha_{\mathrm{s},0,\mathrm{Z}_i}$ and the sorption layer coverage θ_{s}, which is given by the sum of the fractional surface coverage of all competing adsorbate species (i.e. H_2O) $\theta_{\mathrm{s},\mathrm{Z}_p}$.

$$\alpha_{\mathrm{s},\mathrm{Z}_i} = \alpha_{\mathrm{s},0,\mathrm{Z}_i}(1-\theta_{\mathrm{s}}) = \alpha_{\mathrm{s},0,\mathrm{Z}_i}(1-\Sigma\theta_{\mathrm{s},\mathrm{Z}_p}) \quad (22)$$

$\theta_{\mathrm{s},\mathrm{Z}_p}$ is the ratio between the actual and the maximum surface concentration value of Z_p: $\theta_{\mathrm{s},\mathrm{Z}_p} = [\mathrm{Z}_p]_{\mathrm{s}}/[\mathrm{Z}_p]_{\mathrm{s,max}} = \sigma_{\mathrm{s},\mathrm{Z}_p}[\mathrm{Z}_p]_{\mathrm{s}}$, where $\sigma_{\mathrm{s},\mathrm{Z}_p}$ is the effective molecular cross section of Z_p. The inverse molecular cross section can be regarded as the overall concentration of non-interfering sorption sites on the quasi-static surface layer (Pöschl et al., 2007): $[\mathrm{SS}]_{\mathrm{ss}} = \sigma_{\mathrm{s},\mathrm{Z}_p}^{-1}$.

The adsorbed molecules can thermally desorb back to the gas phase. Desorption (the inverse of adsorption) can be described by a first-order rate coefficient $k_{\mathrm{d},\mathrm{Z}_i}$, which is assumed to be independent on $\theta_{\mathrm{s},\mathrm{Z}_i}$. The flux of desorption of gas molecules on the quasi-static particle surface can be expressed using the desorption coefficient $k_{\mathrm{d},\mathrm{Z}_i}$ as

$$J_{\mathrm{des},\mathrm{Z}_i} = k_{\mathrm{d},\mathrm{Z}_i}[\mathrm{Z}_i]_{\mathrm{s}} = \tau_{\mathrm{d},\mathrm{Z}_i}^{-1}[\mathrm{Z}_i]_{\mathrm{s}} \quad (23)$$

The desorption lifetime $\tau_{\mathrm{d},\mathrm{Z}_i}$ is the mean residence time on the surface in the absence of surface reaction and surface-bulk transport.

The transport of semi-volatile species Z_i between sorption layer and quasi-static surface layer ($J_{\mathrm{s,ss},\mathrm{Z}_i}$ and $J_{\mathrm{ss,s},\mathrm{Z}_i}$) are described as follows:

$$J_{\mathrm{s,ss},\mathrm{Z}_i} = k_{\mathrm{s,ss},\mathrm{Z}_i}[\mathrm{Z}_i]_{\mathrm{s}} \quad (24)$$

$$J_{\mathrm{ss,s},\mathrm{Z}_i} = k_{\mathrm{ss,s},\mathrm{Z}_i}[\mathrm{Z}_i]_{\mathrm{ss}} \quad (25)$$

whereas $k_{\mathrm{s,ss},\mathrm{Z}_i}$ and $k_{\mathrm{ss,s},\mathrm{Z}_i}$ are the first-order transport rate coefficients. Estimates for $k_{\mathrm{ss,s},\mathrm{Z}_i}$ can be derived from the corresponding bulk diffusion coefficients $D_{\mathrm{b},\mathrm{Z}_i}$ based on Fick's first law of diffusion considering that a molecule Z_i in the sorption layer needs to travel a distance of δ_{Z_i} to move into the quasi-static surface layer:

$$k_{\mathrm{ss,s},\mathrm{Z}_i} \approx D_{\mathrm{b},\mathrm{Z}_i}/{\delta_{\mathrm{Z}_i}}^2 \quad (26)$$

An estimate for $k_{\mathrm{s,ss},\mathrm{Z}_i}$ can be determined considering mass transport equilibrium conditions. Mass balance implies that $k_{\mathrm{s,ss},\mathrm{Z}_i}[\mathrm{Z}_i]_{\mathrm{s,eq}} = k_{\mathrm{ss,s},\mathrm{Z}_i}[\mathrm{Z}_i]_{\mathrm{bs,eq}}$ ($J_{\mathrm{s,ss},\mathrm{Z}_i} = J_{\mathrm{ss,s},\mathrm{Z}_i}$) and $k_{\mathrm{d},\mathrm{Z}_i}[\mathrm{Z}_i]_{\mathrm{s,eq}} = k_{\mathrm{a},\mathrm{Z}_i}[\mathrm{Z}_i]_{\mathrm{g,eq}}$($J_{\mathrm{des},\mathrm{Z}_i} = J_{\mathrm{ads},\mathrm{Z}_i}$), where $[\mathrm{Z}_i]_{\mathrm{g,eq}}$, $[\mathrm{Z}_i]_{\mathrm{s,eq}}$, and $[\mathrm{Z}_i]_{\mathrm{ss,eq}}$ are the equilibrium or solubility saturation number concentrations of Z_i in the gas phase, on the sorption layer, and in the quasi-static surface layer, respectively. It leads to

$$k_{\mathrm{s,ss},\mathrm{Z}_i} \approx k_{\mathrm{ss,s},\mathrm{Z}_i}\frac{k_{\mathrm{d},\mathrm{Z}_i}[\mathrm{Z}_i]_{\mathrm{ss,eq}}}{k_{\mathrm{a},\mathrm{Z}_i}[\mathrm{Z}_i]_{\mathrm{g,eq}}} \quad (27)$$

Note that $k_{\mathrm{s,ss},\mathrm{Z}_i}$ reflects the vapor pressure of Z_i (p_{Z_i}) as $[\mathrm{Z}_i]_{\mathrm{g,eq}}$ is a function of p_{Z_i} as described in Sect. 2.4.

General rate equations of chemical production and loss by surface layer reactions, which can proceed within the sorption layer (SLR; $P_{\mathrm{s},\mathrm{Z}_i} - L_{\mathrm{s},\mathrm{Z}_i}$), within the quasi-static surface layer (QSLR; $P_{\mathrm{ss},\mathrm{Z}_i} - L_{\mathrm{ss},\mathrm{Z}_i}$), and between reactants of the sorption layer and of the quasi-static layer (SQSLR; $P_{\mathrm{s,ss},\mathrm{Z}_i} - L_{\mathrm{s,ss},\mathrm{Z}_i}$), are given by:

$$P_{\mathrm{s},\mathrm{Z}_i} - L_{\mathrm{s},\mathrm{Z}_i} = \sum_{\nu}\sum_{p}\sum_{q} c_{\mathrm{SLR}\nu,\mathrm{s},\mathrm{Z}_i}[\mathrm{Z}_p]_{\mathrm{s}}\left(k_{\mathrm{SLR}\nu,\mathrm{Z}_p} + k_{\mathrm{SLR}\nu,\mathrm{Z}_p,\mathrm{Z}_q}[\mathrm{Z}_q]_{\mathrm{s}}\right) \quad (28)$$

$$P_{\mathrm{ss},\mathrm{Z}_i} - L_{\mathrm{ss},\mathrm{Z}_i} = \sum_{\nu}\sum_{p}\sum_{q} c_{\mathrm{QSLR}\nu,\mathrm{ss},\mathrm{Z}_i}[\mathrm{Z}_p]_{\mathrm{ss}}\left(k_{\mathrm{QSLR}\nu,\mathrm{Z}_p} + k_{\mathrm{QSLR}\nu,\mathrm{Z}_p,\mathrm{Z}_q}[\mathrm{Z}_q]_{\mathrm{ss}}\right) \quad (29)$$

$$P_{s,ss,Z_i} - L_{s,ss,Z_i} = \sum_{v} \sum_{p} \sum_{q} c_{SQSLRv,ss,Z_i} k_{SQSLRv,Z_p,Z_q} [Z_p]_s [Z_q]_{ss} \quad (30)$$

Here c_{SLRv,s,Z_i}, c_{QSLRv,ss,Z_i} and c_{SQSLRv,ss,Z_i} stand for the stoichiometric coefficients (negative for starting materials and positive for reaction products) of species Z_i in surface reactions ($v = 1, ..., v_{max}$) in a system with a total number of v_{max} (photo-)chemical reactions occurring on the surface of the investigated aerosol particles. k_{SLRv,Z_p} and k_{QSLRv,Z_p} are first-order reaction rate coefficients at sorption and quasi-static surface layer, respectively. k_{SLRv,Z_p,Z_q}, k_{QSLRv,Z_p,Z_q} and k_{SQSLRv,Z_p,Z_q} are second-order reaction rate coefficients.

The quasi-static surface accommodation coefficient (α_{ss,Z_i}), i.e. the probability for an individual gas molecule colliding with the surface to enter the quasi-static surface layer is given by:

$$\alpha_{ss,Z_i} = \alpha_{s,Z_i} \frac{J_{s,ss,Z_i}}{J_{des,Z_i} + J_{s,ss,Z_i} + L_{s,Z_i} + L_{s,ss,Z_i}} \quad (31)$$

2.2 Surface-bulk transport

The surface-bulk transport of semi-volatile species Z_i is defined as exchange between the quasi-static surface layer and near-surface bulk. Based on the PRA framework and following previous studies of kinetic models (Ammann and Pöschl, 2007; Pöschl et al., 2007; Pfrang et al., 2010; Shiraiwa et al., 2010), the quasi-static surface layer to bulk transport flux ($J_{ss,b1,Z_i}$) can be described as:

$$J_{ss,b1,Z_i} = k_{ss,b1,Z_i} [Z_i]_{ss} \quad (32)$$

$k_{ss,b1,Z_i}$ is the first-order transport rate coefficient (s^{-1}) of Z_i. In the same way, bulk to surface transport (J_{b,ss,Z_i}) can be described as follows:

$$J_{b1,ss,Z_i} = k_{b1,ss,Z_i} [Z_i]_{bs} \quad (33)$$

k_{b1,ss,Z_i} (cm s^{-1}) is the first-order transport rate coefficient, which can be regarded as an effective transport velocity. k_{b1,ss,Z_i} can be estimated based on Fick's first law of diffusion considering that a molecule Z_i in the near-surface bulk layer needs to travel a distance of $(\delta_{Z_i} + \delta(1))/2$ to move into the quasi-static surface layer:

$$k_{b1,ss,Z_i} \approx 2\, D_{b,Z_i} / (\delta_{Z_i} + \delta(1)) \quad (34)$$

Under equilibrium conditions, mass conservation implies $k_{b1,ss,Z_i}[Z_i]_{b1} = k_{ss,b1,Z_i}[Z_i]_{ss}$ ($J_{b1,ss,Z_i} = J_{ss,b1,Z_i}$) and for pure Z_i the surface and bulk concentrations are given by the inverse of the effective molecular cross section and of the effective molecular volume, respectively: $[Z_i]_{ss} = \delta_{Z_i}^{-2}$ and $[Z_i]_{b1} = \delta_{Z_i}^{-3}$. Thus, we obtain

$$k_{ss,b1,Z_i} \approx k_{b1,ss,Z_i} / \delta_{Z_i} \quad (35)$$

The bulk accomodation coefficient of Z_i (α_{b,Z_i}), the probability for a gas molecule colliding with surface to enter the bulk of the particle, can be derived considering the transport flux of the molecule Z_i from quasi-static surface layer to the inner bulk J_{ss,b,Z_i}. Z_i in the quasi-static surface layer needs to travel δ_{Z_i} to move into the inner bulk.

$$k_{ss,b,Z_i} \approx D_{b,Z_i} / \delta_{Z_i}^2 \quad (36)$$

$$J_{ss,b,Z_i} = k_{ss,b,Z_i} [Z_i]_{ss} \quad (37)$$

Z_i can enter the bulk after the iterative transport between the sorption layer and the quasi-static surface layer. Thus α_{b,Z_i} can be calculated as follow:

$$\begin{aligned} \alpha_{b,Z_i} &= \alpha_{ss,Z_i} \left\{ \Psi_{ss,b} + (\Psi_{ss,s}\, \Psi_{s,ss})\, \Psi_{ss,b} + (\Psi_{ss,s}\, \Psi_{s,ss})^2\, \Psi_{ss,b} + \cdots \right\} \\ &= \alpha_{ss,Z_i}\, \Psi_{ss,b} \lim_{n\to\infty} \sum_{k=0}^{n} (\Psi_{ss,s}\, \Psi_{s,ss})^k \\ &= \alpha_{ss,Z_i}\, \Psi_{ss,b} \lim_{n\to\infty} \frac{1-(\Psi_{ss,s}\, \Psi_{s,ss})^{n+1}}{1-\Psi_{ss,s}\, \Psi_{s,ss}} \\ &\approx \alpha_{ss,Z_i} \frac{\Psi_{ss,b}}{1-\Psi_{ss,s}\, \Psi_{s,ss}} \end{aligned} \quad (38)$$

where $\Psi_{ss,b}$ and $\Psi_{ss,s}$ are the probabilities for Z_i in the quasi-static surface layer to enter the bulk ($\Psi_{ss,b}$) or transport back to the sorption layer ($\Psi_{ss,s}$); $\Psi_{s,ss}$ is the probability for Z_i in the sorption layer to enter the quasi-static surface layer ($\Psi_{s,ss}$):

$$\Psi_{ss,b} = J_{ss,b,Z_i} / (J_{ss,b,Z_i} + J_{ss,s,Z_i} + L_{ss,Z_i} + L_{s,ss,Z_i}) \quad (39)$$

$$\Psi_{ss,s} = J_{ss,s,Z_i} / (J_{ss,b,Z_i} + J_{ss,s,Z_i} + L_{ss,Z_i} + L_{s,ss,Z_i}) \quad (40)$$

$$\Psi_{s,ss} = J_{s,ss,Z_i} / (J_{s,ss,Z_i} + J_{des,Z_i} + L_{s,Z_i} + L_{s,ss,Z_i}) \quad (41)$$

2.3 Bulk diffusion and reaction

Bulk diffusion is explicitly treated in KM-GAP as the mass transport ($J_{bk,bk\pm1}$) from one bulk layer (bulk k) to the next (bulk $k\pm1$). In analogy to surface–bulk mass transport, we describe the mass transport fluxes between different layers of the bulk by first-order rate equations:

$$J_{bk,bk\pm1,Z_i} = k_{b,b,Z_i}(k)[Z_i]_{bk} \quad (42)$$

Estimates for the transport rate coefficients or effective velocities of Z_i from layer k to $k+1$, $k_{b,b,Z_i}(k)$ (cm s^{-1}), can be calculated from the corresponding diffusion coefficients based on Fick's first law of diffusion. For this purpose we assume that each layer is homogeneously mixed (no concentration gradient within a layer), but note that this assumption can effectively be overcome by choosing an adequately large number of bulk layers The average travel distance for molecules moving from layer k to $k+1$ is $(\delta(k) + \delta(k+1))/2$:

$$k_{b,b,Z_i}(k) = 2D_{b,Z_i} / (\delta(k) + \delta(k+1)) \quad (43)$$

Note that KM-SUB had used an alternative approach to estimate a transport velocity which was based on average travel distance of individual molecules, but the approach presented here is more straightforward and also used successfully in another model

study for similar purposes (Zobrist et al., 2011). This treatment of bulk diffusion yields practically the same results (concentration profiles) as the solving of partial differential equations (Smith et al., 2003; Shiraiwa et al., 2010), but it is more flexible and requires no assumptions about interfacial transport. The influence of changing chemical composition of the particle bulk on diffusion can be taken into account by describing D_{b,Z_i} using the obstruction or percolation theory (Pfrang et al., 2011; Shiraiwa et al., 2011a), or from parameterizations of experimental data (Zobrist et al., 2011).

Chemical reactions proceeding within the bulk of a particle are defined as bulk reactions (BR). For simplicity, we assume that all relevant bulk reactions proceed via quasi-elementary steps with straightforward first- or second-order rate dependences on the concentrations within each bulk layer. The following generalized expressions can be used to describe net chemical production (i.e. production minus loss) of bulk species Z_i within the bulk layer k

$$P_{bk,Z_i} - L_{bk,Z_i} = \sum_{\nu} \sum_{p} c_{BR\nu,Z_i} [Z_p]_{bk} \left(k_{BR\nu,Z_p} + \sum_{q} k_{BR\nu,Z_p,Z_q} [Z_q]_{bk} \right) \quad (44)$$

Here $c_{BR\nu,Z_i}$ stands for the stoichiometric coefficients (negative for starting materials and positive for reaction products) of species Z_i in reaction BRν; $\nu = 1, \ldots, \nu_{max}$ in a system with a total number of ν_{max} chemical reactions occurring in the bulk layer k. $k_{BR\nu,Z_p}$ is a first-order reaction rate coefficient and $k_{BR\nu,Z_p,Z_q}$ is a second-order bulk reaction rate coefficient between Z_p and Z_q in the condensed phase bulk of a system with multiple semi-volatile species which can react with each other. In principle, higher-order reactions might also occur in real systems and could be flexibly included in the model. Moreover, the concentration variables in the rate equations could be replaced by activities or corrected by activity coefficients to account for non-ideal concentration dependencies.

2.4 Vapor pressure

The equilibrium (saturation) number concentrations of Z_i in the gas phase $[Z_i]_{g,eq}$ can be calculated using saturation vapor pressure $p_{Z_i}(d_p)$ of semi-volatile species Z_i, which is a function of a particle diameter by the ideal gas equation:

$$[Z_i]_{g,eq} = \frac{P_{Z_i}(d_p)N_A}{RT_s} \quad (45)$$

For water $P_{Z_i}(d_p)$ can be calculated using Köhler theory (Köhler, 1936; Seinfeld and Pandis, 1998):

$$P_{Z_i}(d_p) = p^o(T_s)\exp\left(\frac{4M_{Z_i}\sigma}{RT_s\rho_{Z_i}d_p}\right) - \frac{6n_sM_{Z_i}}{\pi\rho_{Z_i}{d_p}^3} \quad (46)$$

where σ is the solution surface tention, n_s is moles of solute in the particle, and $p^o(T_s)$ is vapor pressure of pure Z_i over flat surface.

$P_{Z_i}(d_p)$ can be also calculated using a single hygroscopicity parameter κ (Petters and Kreidenweis, 2007):

$$P_{Z_i}(d_p) = p^o(T_s)\frac{{d_p}^3 - {d_d}^3}{{d_p}^3 - {d_d}^3(1-\kappa)}\exp\left(\frac{4M_{Z_i}\sigma}{RT_s\rho_{Z_i}d_p}\right) \quad (47)$$

where d_d is a dry diameter of a particle. Note that $P_{Z_i}(d_p)$ is also a function of surface temperature T_s.

2.5 Heat transfer

For water condensation the heat flux Q directed away from a single droplet can be expressed as (Vesala et al., 1997; Winkler et al., 2006):

$$Q = \pi d_p\beta_T(K(T_s) + K(T))(T_s - T) + H_vI \quad (48)$$

where $K(T_s)$ and $K(T)$ correspond to thermal conductivities of the binary mixture of inert gas and water vapor at the droplet surface temperature (T_s) and the ambient gas temperature (T), respectively. I is the mass flux directed away from a single droplet.

$$I = -J_{net}\pi d_p^2 M_w/N_A \quad (49)$$

β_T is the transitional correction factor for heat transfer given by (Vesala et al., 1997; Winkler et al., 2006)

$$\beta_T = \frac{1 + Kn_T}{1 + (4/3\alpha_T + 0.377)Kn_T + 4/3\alpha_T Kn_T^2} \quad (50)$$

Kn_T is the Knudsen number for heat transfer characterized by particle diameter (d_p) and effective mean free path of the dry air molecules (λ_a):

$$Kn_T = 2\lambda_a/d_p = 6D_T/\omega_a d_p \quad (51)$$

where D_T is the thermal diffusivity of air and ω_a is mean thermal velocity of dry air. H_v is the specific enthalpy of moist air:

$$H_v = H_a + xH_w \quad (52)$$

where H_a and H_w are the specific enthalpies of dry air and water vapor, respectively. These can be calculated from the specific heat capacities of dry air ($c_{p,a}$) and water vapor ($c_{p,w}$), respectively:

$$H_a = c_{p,a}T \quad (53)$$

$$H_w = c_{p,w}T + L_w \quad (54)$$

L_w is the latent heat of water vaporization. The humidity ratio x given in units of $g\,g^{-1}$ is the ratio between the actual mass of water vapor present in moist air to the mass of the dry air.

The droplet surface temperature T_s can be obtained from the heat balance equation (Vesala et al., 1997).

$$Q - H_l\, I = 0 \tag{55}$$

$H_l(T_s)$ is the specific enthalpy of the liquid at the droplet surface temperature.

$$H_l = H_v(T_s) - L_w(T_s) \tag{56}$$

Inserting Eqs. (48) and (56) into Eq. (55) yields

$$T_s = T - \frac{L_w I}{\pi d_p \beta_T (K(T) + K(T_s))} \tag{57}$$

Parameter definitions and values are given in Table 1. The ambient temperature (T) can be calculated by the below heat balance equation.

$$\frac{dT}{dt} = \sum^{N_p} \frac{-L_w I}{c_{p,a} M_a + c_{p,w} M_w} \tag{58}$$

The amount of heat released upon chemical reaction (reaction enthalpy) can be of similar magnitude or larger than the heat release upon condensation. Usually, however, the heat release upon reaction of trace gases with aerosol particles proceeds over much longer time scales than the condensation of cloud droplets, because the mass flux is much smaller. Therefore, the heat released by chemical reactions can be efficiently buffered by the ambient gas and does normally not lead to a substantial increase of particle surface temperature. For example, an oleic acid particle with a radius of 200 nm can be oxidized by ozone on the timescale of a minute. If we insert the corresponding average rate of heat release for $L_w I$ in Eq. (57), the temperature change due to reaction is estimated to be below $\sim 10^{-4}$ K as long as the reaction enthalpy is smaller than about $-2000\,\mathrm{kJ\,mol^{-1}}$. Indeed, the reaction enthalpy of oleic acid ozonolysis is estimated to be on the order of -300 to $-700\,\mathrm{kJ\,mol^{-1}}$ based on

published enthalpies of formation for the reaction products (Bond, 2007; NIST, 2011), assuming 1 mol nonanal, 0.5 mol nonanoic acid, and 0.5 mol azelaic acid as reaction products per mole of oleic acid. Even if we consider the complete combustion of oleic acid with a reaction enthalpy of $-11\,161\,\mathrm{kJ\,mol^{-1}}$ (NIST, 2011), this would only lead to a temperature change of less than 10^{-3} K. Thus, we ignore heat transfer effects in the modeling of chemical reactions in Sect. 3.3 below.

3 Model application

To test and demonstrate the applicability of KM-GAP, we applied KM-GAP to three different processes: water condensation (Sect. 3.1), evaporation kinetics of organics (Sect. 3.2), and particle shrinkage due to chemical reactions (Sect. 3.3). In each simulation the KM-GAP results are compared to experimental data available in the literature.

3.1 Condensation of water vapor

We simulated the condensation of water vapor in comparison to experimental data from Winkler et al. (2006). In their experiments, monodisperse Ag particles with a diameter of 9 nm have been used as condensation nuclei and humidified under initial supersaturation of 37.5 % at 268 K and 737 Torr. The particle number concentration was $4381\,\mathrm{cm^{-3}}$. The growth of water droplet was observed as shown in Fig. 2a.

We modeled the temporal variation of particle radius and surface and ambient temperature by numerically solving the differential equations of mass balance for each model compartment with Matlab software. The model simulations were performed with $n = 50$ bulk layers. The thermodynamic and kinetic parameters required for the simulations are summarized in Table 1. The thermal accommodation coefficient of water ($\alpha_{T,w}$) is reported to be 1 (Winkler et al., 2004). The bulk diffusion coefficient of water ($D_{b,w}$) of supercooled water is reported to be $2 \times 10^{-6}\,\mathrm{cm^2\,s^{-1}}$ at ~268 K (Debenedetti, 1996). The desorption lifetime of water ($\tau_{d,w}$) is estimated to be 3.5×10^{-11} s by the

molecular dynamic simulation (Vieceli et al., 2005; Garrett et al., 2006). $\alpha_{s,0,w}$ is reported to be in the range of 0.1–1 (Davidovits et al., 2004 and references therein), which we varied in this range to fit the experimental data. For simplicity the parameters were assumed to be constant throughout each model run.

Note that the molecular dynamic simulations suggest the air/water interface thickness of 0.3–0.6 nm (Garrett et al., 2006), which is equivalent to approximately two water molecules. At the interface each water molecule has on average two less hydrogen bond than it would have in the bulk (Taylor et al., 1996). KM-GAP captures this interface with monolayers of sorption and quasi-static surface layer.

As shown in Fig. 2b, the simulated temperature of the droplet surface increased to 270 K because of latent heat release by water condensation at the surface. The released heat was then transferred to ambient air, leading to the gradual increase of ambient air temperature. The red lines in Fig. 2a illustrate the model results of KM-GAP with different $\alpha_{s,0,w}$. When $\alpha_{s,0,w}$ of 1 was used (solid line), the simulated line was in very good agreement with the growth observed experimentally, suggesting our best estimate of surface accommodation coefficient of 1 which is consistent with previous experimental and molecular dynamic simulation studies (Morita et al., 2004; Winkler et al., 2004; Garrett et al., 2006). $\alpha_{s,0,w}$ is a critical parameter for cloud modeling, as this value is critical for estimating the number concentration of activated cloud droplets (Laaksonen et al., 2005). The water droplet growth is limited by the gas phase diffusion of water vapor. Due to the continuous water condensation the ambient supersaturation decreased from 37.5 % to ∼33 %. When $\alpha_{s,0,w}$ values between 0.1–0.5 were used, the simulated lines underestimated the growth substantially. In these cases the growth curves were kinetically limited by the surface accommodation of water vapor.

To investigate the effects of bulk diffusion and surface-bulk transport of water, particle growth was simulated with a smaller $D_{b,w}$ value of 10^{-11} cm^2 s^{-1}, which is a characteristic value for ice and other solids (Huthwelker et al., 2006; Shiraiwa et al., 2011a). As illustrated as blue line in Fig. 2a, the particle growth was retarded substantially being kinetically limited by bulk diffusion and surface-bulk transport of water molecules.

The bulk diffusion-limited particle growth may be relevant for condensational growth of amorphous (semi-)solid aerosol particles (Mikhailov et al., 2009; Koop et al., 2011; Tong et al., 2011; Zobrist et al., 2011), which we intend to investigate further in follow-up studies.

3.2 Evaporation of dioctyl phthalate

Here we simulated the size-dependent evaporation of single-component organic particles composed of dioctyl phthalate (DOP) and compare the results to experimental data from Vaden et al. (2011). In their experiments, the monodisperse DOP droplets were loaded into a 7 l evaporation chamber containing 1 l of activated charcoal at the bottom of the chamber which continuously removed gas-phase organics. The number concentration of particles in the chamber was ∼150 cm^{-3} and this value decreased by ∼20 % during the course of the evaporation experiments due to wall losses and dilution during sampling (A. N. Zelenyuk, personal communication, 2011).

We modeled the temporal evolution of particle diameter and gas phase concentration of DOP as a function of evaporation time. The required parameters are: vapor pressure of DOP (10^{-7} Torr) (Cappa et al., 2008); gas phase diffusion coefficient of DOP ($D_{g,DOP} = 4.4 \times 10^{-2}$ cm^2 s^{-1}) (Ray et al., 1988); desorption lifetime of DOP ($\tau_{d,DOP}$) which is assumed to be 10^{-6} s; bulk diffusion coefficient of DOP ($D_{b,DOP} = 3.0 \times 10^{-8}$ cm^2 s^{-1}) which is estimated from the viscosity of DOP (0.081 Pa s) through the Stokes-Einstein equation (Shiraiwa et al., 2011a), using an effective molecular radius of DOP ($\delta_{DOP} = 0.86$ nm) calculated by density ($\rho_{DOP} = 0.986$ g cm^{-3}) and molar mass ($M_{DOP} = 390.56$ g mol^{-1}). The surface accommodation coefficient of DOP on free substrate ($\alpha_{s,0,DOP}$) is varied to fit to the data. The loss of DOP to the denuder is considered with the simple assumption that assuming that the core of the chamber is well-mixed and the loss occurs via molecular diffusion (1st Fick's law) through a layer adjacent to the denuder wall. We varied the thickness of the denuder wall up to the half-height of the chamber (∼3 cm).

The experimentally measured size- and time-dependent evaporation of DOP is modeled well by KM-GAP as shown in Fig. 3, in which molecular diffusion distance for denuder loss is assumed to be the half-height of the chamber and $\alpha_{s,0,DOP}$ of 0.5. The modeled gas phase concentration of DOP is $\sim 10^9$ cm^{-3} mainly determined by the vapor pressure of DOP. Due to turbulent mixing in the chamber, the actual molecular diffusion distance might be smaller (Crump and Seinfeld, 1981). For example, the data can be also reproduced with smaller diffusion distance of 1 mm and $\alpha_{s,0,DOP}$ of ~0.3, while variations of $\tau_{d,DOP}$ showed practically no effect, which emphasizes the importance of mixing effects and chamber geometry. This information and related model sensitivity studies can be used to design and optimize further experiments for efficient probing of specific physical effects (e.g. experiments with variable chamber geometry to probe accommodation vs. mixing).

For the above modeling the particle number concentration was kept constant at the initial concentration for simplicity. The sensitivity studies on particle number concentration showed that a particle loss of 20 % during the course of the experiments does not affect the evaporation behavior significantly. If the number concentration is decreased by factor of 10, however, the particles shrink faster by ~5 % because of lower gas phase concentration of DOP, suggesting that the particle number concentration also plays a role in such evaporation experiments. While traditional evaporation models may suffice to describe simple systems consisting of single components or liquid droplets, KM-GAP may provide further insight into the interplay of mass transport, phase transitions and chemical reactions in complex multi-component systems of variable composition and phase state such as (secondary) organic aerosols that undergo chemical aging and transformation (Cappa and Wilson, 2011; Pfrang et al., 2011). We intend to investigate the evaporation kinetics of (semi-)solid particles composed of multiple components in follow-up studies.

3.3 Oxidation and volatilization of oleic acid

Here we simulated the degradation of oleic acid by ozone in comparison to experimental data from Ziemann (2005). The same data set has been used by Pfrang et al. (2010) and Shiraiwa et al. (2010) for simulations with a kinetic double-layer model (K2-SUB) and kinetic-multi layer model (KM-SUB) for aerosol surface and bulk chemistry. In those studies the gas-particle partitioning of products was not considered, which is now included in the KM-GAP simulation. The products of oleic acid oxidation by ozone are mainly 1-nonanal, 9-oxononanoic acid, nonanoic acid, azelaic acid, and peroxidic dimer (e.g. Zahardis and Petrucci, 2007; Vesna et al., 2009). Physical properties of oleic acid and its products are summarized in Table 2. The assumed product yield of oleic acid ozonolysis is also given (compare Zahardis and Petrucci, 2007). For simplicity we assume only nonanal is volatile and oleic acid and other products are non-volatile as their vapor pressures are low and all products other than 1-nonanal, 9-oxononanoic acid, nonanoic acid and azelaic acid can be represented by a dimer. We intend to investigate more in detail removing these simpliying assumptions in follow-up studies.

The gas phase ozone concentration was set to $[Z_1]_g = [Z_1]_{gs} = 7.0 \times 10^{13}$ cm^{-3} (corresponding to 2.8 ppm at 1013 hPa and 298 K). The initial surface and bulk concentrations of ozone (Z_1) and nonanal were set to $[Z_i]_{s,0} = [Z_i]_{bk,0} = 0$. The initial surface and bulk concentrations of oleic acid (Z_2) were set to $[Z_2]_{ss,0} = 9.7 \times 10^{13}$ cm^{-2} and $[Z_2]_{b,0} = 1.2 \times 10^{21}$ cm^{-3}, respectively (Pfrang et al., 2010), corresponding to 3.15 mol l^{-1} as reported by Ziemann (2005). Accordingly, the initial value of the total number of oleic acid molecules in a particle with a radius of 0.2 µm was $N_{Z_2,0} = 4.1 \times 10^7$. Note that the bulk concentration of pure oleic acid is actually 1.95×10^{21} cm^{-3} based on molecular weight and density, but the lower value of 1.2×10^{21} cm^{-3} is used as an initial value because oleic acid was already exposed to ozone until ozone is well-mixed in the chamber (Ziemann, 2005). Therefore, oleic acid is already partly degraded and initial concentration of non-volatile products are estimated based on the product yield.

We modeled the temporal evolution of particle size, the particle surface and bulk composition, and of the ozone uptake coefficient by numerically solving the differential equations of mass balance for each model compartment with Matlab software (ode23tb solver with 999 time steps). The kinetic parameters required for the model simulations are based on parameters of base case 1 given in Shiraiwa et al. (2010) and summarized in Table 2: the surface accommodation coefficient of ozone ($\alpha_{s,0,Z_1}$), the desorption lifetime of ozone and nonanal (τ_d), the second-order reaction rate coefficient at surface, quasi-static surface, and bulk ($k_{SLR,Z_1,Z_2} = k_{QSLR,Z_1,Z_2} = 6 \times 10^{-12}$ cm^{-2}; $k_{BR,Z_1,Z_2} = 5 \times 10^{-17}$ cm^{-2}). The bulk diffusion coefficients (D_b) of oleic acid, nonanal, and nonanoic acid were estimated from viscosity data (Noureddini et al., 1992) using the Stokes-Einstein equation (Shiraiwa et al., 2011a). Additional input parameters were the mean thermal velocity of ozone ($\omega_{Z_1} = 3.6 \times 10^4$ cm s^{-1}), the Henry's law coefficient of ozone ($K_{sol,cc,Z_1} = 4.8 \times 10^{-4}$ mol cm^{-3} atm^{-1}) and vapor pressure of nonanal (~0.4 Torr) (Verevkin et al., 2003). For simplicity the kinetic parameters were assumed to be constant throughout each model run.

The model simulations were performed with $n = 100$ layers to obtain the high resolution results of bulk concentration profiles. To test how the number of model layers in the particle bulk affects the simulation results, we have run the model within $n = 5$–200. The model results of oleic acid degradation and particle growth were identical, demonstrating the robustness of the multi-layer model approach with transport rate coefficients scaled by layer thickness (Eqs. 34, 35, 43) (Shiraiwa et al., 2010).

Figure 4 illustrates the model results of KM-GAP. As shown in Fig. 4a, KM-GAP can fit to the simulated decay of oleic acid very well. The particle shrinks with the radius decreasing from 200 nm to 187 nm in 30 s, due to the formation and evaporation of the volatile product (i.e. nonanal). The simulated ozone uptake coefficient is nearly constant and identical to the surface and bulk accommodation coefficients ($\gamma_{Z_1} \approx \alpha_{s,Z_1} \approx \alpha_{ss,Z_1} \approx \alpha_{b,Z_1} \approx 4.2 \times 10^{-4}$), indicating that the gas uptake is limited by interfacial mass transport, i.e. by the process of bulk accommodation which is in turn limited by

the process of surface accommodation. Note that even if evaporation of nonanal is switched off (i.e. no particle shrinkage) the oleic acid degradation is well reproduced by KM-GAP with the same kinetic parameters, indicating the limited impact of evaporation of volatile products on organics degradation in this particular experimental data set.

As shown in Fig. 4b, the surface concentration of ozone at the quasi-static surface layer increases gradually owing to the combination of reversible adsorption, surface reaction, and surface-to-bulk transport driven by the chemical reaction in the bulk. In contrast, the surface concentration of oleic acid decreases due to chemical reaction with ozone and while the concentration of nonvolatile products increases for the same reason. The surface concentration of nonanal stays very low (~10^6 cm^{-2}) at steady-state determined by desorption, chemical production and transport from the bulk. A very similar behavior is observed for the average bulk concentrations as illustrated in Fig. 4c. The bulk concentration of nonanal stays constant at a low level, whereas the concentrations of non-volatile products increase as oleic acid is degraded by bulk reaction.

Figure 5 shows the bulk concentration profiles of (a) ozone, (b) oleic acid, (c) nonanal, and (d) other non-volatile products (i.e. oxononanoic + nonanoic + azelaic acids + dimer). The y-axis displays the radial distance from the particle core. As shown in Fig. 5a, ozone diffuses rapidly into the bulk and a concentration gradient between near-surface bulk and core is observed, which is determined by the interplay of interfacial transport with bulk diffusion and reaction. During the first few seconds, the ozone concentration in the near-surface bulk is almost two orders of magnitude higher than in the particle center, because ozone is depleted due to fast bulk reaction in the near-surface bulk before it can diffuse more deeply into the bulk. Up to ~30 s, the concentration gradient swiftly relaxes with decreasing abundance of oleic acid.

As illustrated in Fig. 5b, the strong concentration gradient of ozone induces almost no gradient for oleic acid because the concentration of oleic acid is ~8 orders of magnitude higher than that of ozone (Fig. 4c). Thus, oleic acid can effectively be regarded as well-mixed (i.e. concentration differences <1 %). Figure 5c illustrates the bulk concentration

profile of nonanal. It is interesting to note that even though the average bulk concentration of nonanal stays constant at a low concentration level ($\sim 10^{14}$ cm^{-3}) as shown in Fig. 4c, a concentration gradient is observed. The concentration at the core is by factor of ~5 higher than that in the near-surface bulk for the first 20 s, when the evaporation rate of nonanal is faster than bulk diffusion, which in turn is faster than the chemical production rate. After ~20 s, when ozone reaches the particle core, the production rate of nonanal becomes faster than bulk diffusion leading to a steeper concentration gradient. In contrast, non-volatile products show only a small concentration gradients, but at a high concentration level ($\sim 10^{21}$ cm^{-3}).

4 Summary and conclusions

We present a novel kinetic multi-layer model of gas-particle interactions in aerosols and clouds (KM-GAP) that treats explicitly all steps of mass transport and chemical reaction of semi-volatile species partitioning between gas phase, particle surface and particle bulk. KM-GAP builds on the kinetic multi-layer model for aerosol surface and bulk chemistry which includes gas phase diffusion, reversible adsorption, surface reactions, and bulk diffusion and reaction (KM-SUB; Shiraiwa et al., 2010). The new processes included in KM-GAP are heat flux, evaporation and condensation of semi-volatile species. The size change of the particle and the temporal evolution and concentration profiles of semi-volatile species at the gas-particle interface as well as in the particle bulk can be modeled along with surface concentrations and gas uptake coefficients. Depending on the complexity of the investigated system, unlimited numbers of semi-volatile species, chemical reactions, and physical processes can be treated, and the model shall help to bridge gaps in the understanding and quantification of multiphase chemistry and microphysics in atmospheric aerosols and clouds.

To demonstrate the applicability of KM-GAP, the condensation of water vapor on nanoparticles was simulated and compared to experimental data. Resolving the reversible adsorption of water vapor with a water desorption lifetime of picoseconds as

suggested by molecular dynamic simulations, we confirm the best estimate of the surface accommodation coefficient of water vapor on a water droplet to be unity. Sensitivity studies suggest that an artificially slow bulk diffusion can inhibit the particle growth significantly, which may be relevant for condensational growth of (semi-)solid organic aerosol particles.

For further demonstration of the ability of KM-GAP, the size- and time-dependent evaporation of single organic component particles was modeled. Experimental data on the evaporation of dioctyl phthalate particles can be reproduced with an accommodation coefficient of ~0.5, and the model results emphasize the importance of aerosol particle number concentration and mixing effects in chamber experiments. Moreover, we showed how the formation and evaporation of volatile reaction products like nonanal can cause a decrease in the size of oleic acid particles exposed to ozone.

In conclusion, KM-GAP is a versatile tool for the modeling of multiphase chemical and microphysical processes in atmospheric aerosols and clouds in a self-consistent and realistic manner. The model can resolve the effects of surface and bulk mass transport in particles undergoing condensation and/or evaporation, which may be crucial for the description and understanding of the atmospheric aging of multi-component mixtures of time-dependent composition and diffusivity. So far the formation and aging of secondary organic aerosol (SOA) has generally been described by thermodynamic models that implicitly assume quasi-instantaneous gas-particle partitioning (Pankow, 1994; Donahue et al., 2006; Zuend et al., 2010; Donahue et al., 2011). If, however, the phase state of SOA is not liquid but (semi-)solid, this assumption may break down and the SOA partitioning may be kinetically limited (Virtanen et al., 2010; Cappa and Wilson, 2011; Shiraiwa et al., 2011; Vaden et al., 2011). We suggest and intend to use KM-GAP for the investigation of such effects.

Acknowledgements. Corresponding authorship is shared by M. Shiraiwa (m.shiraiwa@mpic.de) and U. Pöschl (u.poschl@mpic.de). This work was funded by the Max Planck Society (MPG) and the European Commission under the projects EUCAARI (grant no. 036833-2) and PEGASOS (grant no. 265148). MS was supported by the Max Planck

Graduate Center (MPGC) – Johannes Gutenberg University Mainz (JOGU) and the Ministry of Education, Culture, Sports, Science and Technology – Japan (MEXT). CP wishes to thank the Royal Society, NERC (grant no. NE/G000883/1) and the University of Reading for support for his collaboration with the Max Planck Institute for Chemistry. We thank U. K. Krieger, B. P. Luo, M. Ammann, T. Peter, A. J. Huisman, H. Su, I. Riipinen, and J. H. Seinfeld for stimulating discussions and A. N. Zelenyuk for sharing information about DOP evaporation experiments.

The service charges for this open access publication
have been covered by the Max Planck Society.

References

Ammann, M. and Pöschl, U.: Kinetic model framework for aerosol and cloud surface chemistry and gas-particle interactions – Part 2: Exemplary practical applications and numerical simulations, Atmos. Chem. Phys., 7, 6025–6045, doi:10.5194/acp-7-6025-2007, 2007.

Andreae, M. O. and Crutzen, P. J.: Atmospheric aerosols: Biogeochemical sources and role in atmospheric chemistry, Science, 276, 1052–1058, doi:10.1126/science.276.5315.1052, 1997.

Andreae, M. O. and Rosenfeld, D.: Aerosol-cloud-precipitation interactions. Part 1. The nature and sources of cloud-active aerosols, Earth-Sci. Rev., 89, 13–41, doi:10.1016/j.earscirev.2008.03.001, 2008.

Anttila, T., Kiendler-Scharr, A., Tillmann, R., and Mentel, T. F.: On the reactive uptake of gaseous compounds by organic-coated aqueous aerosols: Theoretical analysis and application to the heterogeneous hydrolysis of N_2O_5, J. Phys. Chem. A, 110, 10435–10443, doi:10.1021/jp062403c, 2006.

Bond, D.: Computational methods in organic thermochemistry. 2. Enthalpies and free energies of formation for functional derivatives of organic hydrocarbons, J. Organic Chem., 72, 7313–7328, doi:10.1021/jo071213a, 2007.

Cappa, C. D. and Wilson, K. R.: Evolution of organic aerosol mass spectra upon heating: implications for OA phase and partitioning behavior, Atmos. Chem. Phys., 11, 1895–1911, doi:10.5194/acp-11-1895-2011, 2011.

Cappa, C. D., Lovejoy, E. R., and Ravishankara, A. R.: Evaporation Rates and Vapor Pressures

of the Even-Numbered C8-C18 Monocarboxylic Acids, J. Phys. Chem. A, 112, 3959–3964, doi:10.1021/jp710586m, 2008.

Crump, J. G. and Seinfeld, J. H.: Turbulent deposition and gravitational sedimentation of an aerosol in a vessel of arbitrary shape, J. Aerosol Sci., 12, 405–415, doi:10.1016/0021-8502(81)90036-7, 1981.

Davidovits, P., Worsnop, D. R., Jayne, J. T., Kolb, C. E., Winkler, P., Vrtala, A., Wagner, P. E., Kulmala, M., Lehtinen, K. E. J., Vesala, T., and Mozurkewich, M.: Mass accommodation coefficient of water vapor on liquid water, Geophys. Res. Lett., 31, L22111, doi:10.1029/2004gl020835, 2004.

Debenedetti, P. G.: Metastable liquids: concepts and principles, Princeton University Press, Princeton, 1996.

Donahue, N. M., Robinson, A. L., Stanier, C. O., and Pandis, S. N.: Coupled partitioning, dilution, and chemical aging of semivolatile organics, Environ. Sci. Technol., 40, 02635–02643, doi:10.1021/es052297c, 2006.

Donahue, N. M., Epstein, S. A., Pandis, S. N., and Robinson, A. L.: A two-dimensional volatility basis set: 1. organic-aerosol mixing thermodynamics, Atmos. Chem. Phys., 11, 3303–3318, doi:10.5194/acp-11-3303-2011, 2011.

Finlayson-Pitts, B. J. and Pitts, J. N.: Tropospheric air pollution: Ozone, airborne toxics, polycyclic aromatic hydrocarbons, and particles, Science, 276, 1045–1052, doi:10.1126/science.276.5315.1045, 1997.

Fry, J. L., Kiendler-Scharr, A., Rollins, A. W., Brauers, T., Brown, S. S., Dorn, H.-P., Dubé, W. P., Fuchs, H., Mensah, A., Rohrer, F., Tillmann, R., Wahner, A., Wooldridge, P. J., and Cohen, R. C.: SOA from limonene: role of NO_3 in its generation and degradation, Atmos. Chem. Phys., 11, 3879–3894, doi:10.5194/acp-11-3879-2011, 2011.

Garrett, B. C., Schenter, G. K. and Morita, A.: Molecular simulations of the transport of molecules across the liquid/vapor interface of water, Chem. Rev., 106, 1355–1374, doi:10.1021/cr040370w, 2006.

George, I. J. and Abbatt, J. P. D.: Chemical evolution of secondary organic aerosol from OH-initiated heterogeneous oxidation, Atmos. Chem. Phys., 10, 5551–5563, doi:10.5194/acp-10-5551-2010, 2010a.

George, I. J. and Abbatt, J. P. D.: Heterogeneous oxidation of atmospheric aerosol particles by gas-phase radicals, Nature Chem., 2, 713–722, doi:10.1038/nchem.806, 2010b.

Hallquist, M., Wenger, J. C., Baltensperger, U., Rudich, Y., Simpson, D., Claeys, M., Dommen,

J., Donahue, N. M., George, C., Goldstein, A. H., Hamilton, J. F., Herrmann, H., Hoffmann, T., Iinuma, Y., Jang, M., Jenkin, M. E., Jimenez, J. L., Kiendler-Scharr, A., Maenhaut, W., McFiggans, G., Mentel, Th. F., Monod, A., Prévôt, A. S. H., Seinfeld, J. H., Surratt, J. D., Szmigielski, R., and Wildt, J.: The formation, properties and impact of secondary organic aerosol: current and emerging issues, Atmos. Chem. Phys., 9, 5155–5236, doi:10.5194/acp-9-5155-2009, 2009.

Hanson, D. R.: Surface-specific reactions on liquids, J. Phys. Chem. B, 101, 4998–5001, 1997.

Huthwelker, T., Ammann, M., and Peter, T.: The uptake of acidic gases on ice, Chem. Rev., 106, 1375–1444, doi:10.1021/cr020506v, 2006.

Ivanov, A. V., Trakhtenberg, S., Bertram, A. K., Gershenzon, Y. M., and Molina, M. J.: OH, HO_2, and ozone gaseous diffusion coefficients, J. Phys. Chem. A, 111, 1632–1637, doi:10.1021/jp066558w, 2007.

Jimenez, J. L., Canagaratna, M. R., Donahue, N. M., Prevot, A. S. H., Zhang, Q., Kroll, J. H., DeCarlo, P. F., Allan, J. D., Coe, H., Ng, N. L., Aiken, A. C., Docherty, K. S., Ulbrich, I. M., Grieshop, A. P., Robinson, A. L., Duplissy, J., Smith, J. D., Wilson, K. R., Lanz, V. A., Hueglin, C., Sun, Y. L., Tian, J., Laaksonen, A., Raatikainen, T., Rautiainen, J., Vaattovaara, P., Ehn, M., Kulmala, M., Tomlinson, J. M., Collins, D. R., Cubison, M. J., Dunlea, E. J., Huffman, J. A., Onasch, T. B., Alfarra, M. R., Williams, P. I., Bower, K., Kondo, Y., Schneider, J., Drewnick, F., Borrmann, S., Weimer, S., Demerjian, K., Salcedo, D., Cottrell, L., Griffin, R., Takami, A., Miyoshi, T., Hatakeyama, S., Shimono, A., Sun, J. Y., Zhang, Y. M., Dzepina, K., Kimmel, J. R., Sueper, D., Jayne, J. T., Herndon, S. C., Trimborn, A. M., Williams, L. R., Wood, E. C., Middlebrook, A. M., Kolb, C. E., Baltensperger, U., and Worsnop, D. R.: Evolution of Organic Aerosols in the Atmosphere, Science, 326, 1525–1529, doi:10.1126/science.1180353, 2009.

Kaiser, J. C., Riemer, N., and Knopf, D. A.: Detailed heterogeneous oxidation of soot surfaces in a particle-resolved aerosol model, Atmos. Chem. Phys., 11, 4505–4520, doi:10.5194/acp-11-4505-2011, 2011.

Kalberer, M., Paulsen, D., Sax, M., Steinbacher, M., Dommen, J., Prevot, A. S. H., Fisseha, R., Weingartner, E., Frankevich, V., Zenobi, R., and Baltensperger, U.: Identification of polymers as major components of atmospheric organic aerosols, Science, 303, 1659–1662, 2004.

King, M. D., Rennie, A. R., Thompson, K. C., Fisher, F. N., Dong, C. C., Thomas, R. K., Pfrang, C., and Hughes, A. V.: Oxidation of oleic acid at the air-water interface and its potential effects on cloud critical supersaturations, Phys. Chem. Chem. Phys., 11, 7699–7707,

doi:10.1039/b906517b, 2009.

Knopf, D. A., Anthony, L. M., and Bertram, A. K.: Reactive uptake of O_3 by multicomponent and multiphase mixtures containing oleic acid, J. Phys. Chem. A, 109, 5579–5589, 2005.

Köhler, H.: The nucleus in and the growth of hygroscopic droplets, Trans. Faraday Soc., 32, 1152–1161, 1936.

Kolb, C. E., Cox, R. A., Abbatt, J. P. D., Ammann, M., Davis, E. J., Donaldson, D. J., Garrett, B. C., George, C., Griffiths, P. T., Hanson, D. R., Kulmala, M., McFiggans, G., Pöschl, U., Riipinen, I., Rossi, M. J., Rudich, Y., Wagner, P. E., Winkler, P. M., Worsnop, D. R., and O' Dowd, C. D.: An overview of current issues in the uptake of atmospheric trace gases by aerosols and clouds, Atmos. Chem. Phys., 10, 10561–10605, doi:10.5194/acp-10-10561-2010, 2010.

Koop, T., Luo, B. P., Tsias, A., and Peter, T.: Water activity as the determinant for homogeneous ice nucleation in aqueous solutions, Nature, 406, 611–614, doi:10.1038/35020537, 2000.

Koop, T., Bookhold, J., Shiraiwa, M., and Pöschl, U.: Glass transition and phase state of organic compounds: dependency on molecular properties and implications for secondary organic aerosols in the atmosphere, Phys. Chem. Chem. Phys., 13, 19238–19255, 2011.

Kuwata, M., Chen, Q., and Martin, S. T.: Cloud condensation nuclei (CCN) activity and oxygen-to-carbon elemental ratios following thermodenuder treatment of organic particles grown by alpha-pinene ozonolysis, Phys. Chem. Chem. Phys., 13, 14571–14583, doi:10.1039/c1cp20253g, 2011.

Laaksonen, A., Vesala, T., Kulmala, M., Winkler, P. M. and Wagner, P. E.: Commentary on cloud modelling and the mass accommodation coefficient of water, Atmos. Chem. Phys., 5, 461-464, 10, http://www.atmos-chem-phys.net/5/461/10/.5194/acp-5-461-2005, 2005.

Loza, C. L., Chhabra, P. S., Yee, L. D., Craven, J. S., Flagan, R. C., and Seinfeld, J. H.: Chemical aging of m-xylene secondary organic aerosol: laboratory chamber study, Atmos. Chem. Phys. Discuss., 11, 24969–25010, doi:10.5194/acpd-11-24969-2011, 2011.

Lu, J. W., Flores, J. M., Lavi, A., Abo-Riziq, A., and Rudich, Y.: Changes in the optical properties of benzo a pyrene-coated aerosols upon heterogeneous reactions with NO_2 and NO_3, Phys. Chem. Chem. Phys., 13, 6484–6492, doi:10.1039/c0cp02114h, 2011.

Marcolli, C., Luo, B. P., and Peter, T.: Mixing of the organic aerosol fractions: Liquids as the thermodynamically stable phases, J. Phys. Chem. A, 108, 2216–2224, doi:10.1021/jp036080l, 2004.

McNeill, V. F., Yatavelli, R. L. N., Thornton, J. A., Stipe, C. B., and Landgrebe, O.: Heterogeneous OH oxidation of palmitic acid in single component and internally mixed aerosol particles: vaporization and the role of particle phase, Atmos. Chem. Phys., 8, 5465–5476, doi:10.5194/acp-8-5465-2008, 2008.

Mikhailov, E., Vlasenko, S., Martin, S. T., Koop, T., and Pöschl, U.: Amorphous and crystalline aerosol particles interacting with water vapor: conceptual framework and experimental evidence for restructuring, phase transitions and kinetic limitations, Atmos. Chem. Phys., 9, 9491–9522, doi:10.5194/acp-9-9491-2009, 2009.

Moise, T. and Rudich, Y.: Reactive uptake of ozone by proxies for organic aerosols: Surface versus bulk processes, J. Geophys. Res.-Atmos., 105, 14667–14676, 2000.

Morita, A., Sugiyama, M., Kameda, H., Koda, S., and Hanson, D. R.: Mass accommodation coefficient of water: Molecular dynamics simulation and revised analysis of droplet train/flow reactor experiment, J. Phys. Chem. B, 108, 9111–9120, doi:10.1021/jp030479s, 2004.

Murray, B. J., Wilson, T. W., Dobbie, S., Cui, Z. Q., Al-Jumur, S., Mohler, O., Schnaiter, M., Wagner, R., Benz, S., Niemand, M., Saathoff, H., Ebert, V., Wagner, S., and Karcher, B.: Heterogeneous nucleation of ice particles on glassy aerosols under cirrus conditions, Nat. Geosci., 3, 233–237, doi:10.1038/ngeo817, 2010.

Nash, D. G., Tolocka, M. P., and Baer, T.: The uptake of O_3 by myristic acid-oleic acid mixed particles: evidence for solid surface layers, Phys. Chem. Chem. Phys., 8, 4468–4475, doi:10.1039/b609855j, 2006.

Noureddini, H., Teoh, B. C., and Clements, L. D.: Viscosities of vegetable-oils and fatty-acids, Journal of the American Oil Chemists Society, 69, 1189–1191, doi:10.1007/bf02637678, 1992.

Odum, J. R., Hoffmann, T., Bowman, F., Collins, D., Flagan, R. C., and Seinfeld, J. H.: Gas/particle partitioning and secondary organic aerosol yields, Environ. Sci. Technol., 30, 2580–2585, 1996.

Pankow, J. F.: An absorption-model of the gas aerosol partitioning involved in the formation of secondary organic aerosol, Atmos. Environ., 28, 189–193, 1994.

Petters, M. D. and Kreidenweis, S. M.: A single parameter representation of hygroscopic growth and cloud condensation nucleus activity, Atmos. Chem. Phys., 7, 1961–1971, doi:10.5194/acp-7-1961-2007, 2007.

Pfrang, C., Shiraiwa, M., and Pöschl, U.: Coupling aerosol surface and bulk chemistry with a kinetic double layer model (K2-SUB): oxidation of oleic acid by ozone, Atmos. Chem. Phys.,

10, 4537–4557, doi:10.5194/acp-10-4537-2010, 2010.

Pfrang, C., Shiraiwa, M., and Pöschl, U.: Chemical ageing and transformation of diffusivity in semi-solid multi-component organic aerosol particles, Atmos. Chem. Phys., 11, 7343–7354, doi:10.5194/acp-11-7343-2011, 2011.

Pöschl, U.: Atmospheric aerosols: Composition, transformation, climate and health effects, Angew. Chem.-Int. Edit., 44, 7520–7540, doi:10.1002/anie.200501122, 2005.

Pöschl, U., Rudich, Y., and Ammann, M.: Kinetic model framework for aerosol and cloud surface chemistry and gas-particle interactions – Part 1: General equations, parameters, and terminology, Atmos. Chem. Phys., 7, 5989–6023, doi:10.5194/acp-7-5989-2007, 2007.

Pöschl, U., Martin, S. T., Sinha, B., Chen, Q., Gunthe, S. S., Huffman, J. A., Borrmann, S., Farmer, D. K., Garland, R. M., Helas, G., Jimenez, J. L., King, S. M., Manzi, A., Mikhailov, E., Pauliquevis, T., Petters, M. D., Prenni, A. J., Roldin, P., Rose, D., Schneider, J., Su, H., Zorn, S. R., Artaxo, P., and Andreae, M. O.: Rainforest Aerosols as Biogenic Nuclei of Clouds and Precipitation in the Amazon, Science, 329, 1513–1516, doi:10.1126/science.1191056, 2010.

Ray, A. K., Lee, J., and Tilley, H. L.: Direct measurements of evaporation rates of single droplets at large Knudsen numbers, Langmuir, 4, 631–637, doi:10.1021/la00081a023, 1988.

Renbaum, L. H. and Smith, G. D.: The importance of phase in the radical-initiated oxidation of model organic aerosols: reactions of solid and liquid brassidic acid particles, Phys. Chem. Chem. Phys., 11, 2441–2451, 10.1039/b816799k, 2009.

Riipinen, I., Pierce, J. R., Yli-Juuti, T., Nieminen, T., Häkkinen, S., Ehn, M., Junninen, H., Lehtipalo, K., Petäjä, T., Slowik, J., Chang, R., Shantz, N. C., Abbatt, J., Leaitch, W. R., Kerminen, V.-M., Worsnop, D. R., Pandis, S. N., Donahue, N. M., and Kulmala, M.: Organic condensation: a vital link connecting aerosol formation to cloud condensation nuclei (CCN) concentrations, Atmos. Chem. Phys., 11, 3865–3878, doi:10.5194/acp-11-3865-2011, 2011.

Robinson, A. L., Donahue, N. M., Shrivastava, M. K., Weitkamp, E. A., Sage, A. M., Grieshop, A. P., Lane, T. E., Pierce, J. R., and Pandis, S. N.: Rethinking organic aerosols: Semivolatile emissions and photochemical aging, Science, 315, 1259–1262, doi:10.1126/science.1133061, 2007.

Salo, K., Hallquist, M., Jonsson, Å. M., Saathoff, H., Naumann, K.-H., Spindler, C., Tillmann, R., Fuchs, H., Bohn, B., Rubach, F., Mentel, Th. F., Müller, L., Reinnig, M., Hoffmann, T., and Donahue, N. M.: Volatility of secondary organic aerosol during OH radical induced ageing, Atmos. Chem. Phys., 11, 11055–11067, doi:10.5194/acp-11-11055-2011, 2011.

Schwier, A. N., Sareen, N., Lathem, T. L., Nenes, A., and McNeill, V. F.: Ozone oxidation of oleic acid surface films decreases aerosol cloud condensation nuclei activity, J. Geophys. Res.-Atmos., 116, D16202, doi:10.1029/2010jd015520, 2011.

Seinfeld, J. H. and Pandis, S. N.: Atmospheric chemistry and physics - From air pollution to climate change, John Wiley & Sons, Inc., New York, 1998.

Seinfeld, J. H. and Pankow, J. F.: Organic atmospheric particulate material, Annu. Rev. Phys. Chem., 54, 121–140, doi:10.1146/annurev.physchem.54.011002.103756, 2003.

Shiraiwa, M., Garland, R. M., and Pöschl, U.: Kinetic double-layer model of aerosol surface chemistry and gas-particle interactions (K2-SURF): Degradation of polycyclic aromatic hydrocarbons exposed to O_3, NO_2, H_2O, OH and NO_3, Atmos. Chem. Phys., 9, 9571–9586, doi:10.5194/acp-9-9571-2009, 2009.

Shiraiwa, M., Pfrang, C., and Pöschl, U.: Kinetic multi-layer model of aerosol surface and bulk chemistry (KM-SUB): the influence of interfacial transport and bulk diffusion on the oxidation of oleic acid by ozone, Atmos. Chem. Phys., 10, 3673–3691, doi:10.5194/acp-10-3673-2010, 2010.

Shiraiwa, M., Ammann, M., Koop, T., and Pöschl, U.: Gas uptake and chemical aging of semisolid organic aerosol particles, P. Natl. Acad. Sci. USA, 108, 11003–11008, doi:10.1073/pnas.1103045108, 2011a.

Shiraiwa, M., Sosedova, Y., Rouviere, A., Yang, H., Zhang, Y., Abbatt, J. P. D., Ammann, M., and Pöschl, U.: The role of long-lived reactive oxygen intermediates in the reaction of ozone with aerosol particles, Nature Chem., 3, 291–295, doi:10.1038/nchem.988, 2011b.

Smith, G. D., Woods, E., Baer, T., and Miller, R. E.: Aerosol uptake described by numerical solution of the diffusion – Reaction equations in the particle, J. Phys. Chem. A, 107, 9582–9587, doi:10.1021/jp021843a, 2003.

Springmann, M., Knopf, D. A., and Riemer, N.: Detailed heterogeneous chemistry in an urban plume box model: reversible co-adsorption of O_3, NO_2, and H_2O on soot coated with benzo[a]pyrene, Atmos. Chem. Phys., 9, 7461–7479, doi:10.5194/acp-9-7461-2009, 2009.

Taylor, R. S., Dang, L. X., and Garrett, B. C.: Molecular dynamics simulations of the liquid/vapor interface of SPC/E water, J. Phys. Chem., 100, 11720–11725, 1996.

Tong, H.-J., Reid, J. P., Bones, D. L., Luo, B. P., and Krieger, U. K.: Measurements of the timescales for the mass transfer of water in glassy aerosol at low relative humidity and ambient temperature, Atmos. Chem. Phys., 11, 4739–4754, doi:10.5194/acp-11-4739-2011, 2011.

Vaden, T. D., Imre, D., Beranek, J., Shrivastava, M., and Zelenyuk, A.: Evaporation kinetics and phase of laboratory and ambient secondary organic aerosol, P. Natl. Acad. Sci. USA, 108, 2190–2195, doi:10.1073/pnas.1013391108, 2011.

Verevkin, S. P., Krasnykh, E. L., Vasiltsova, T. V., Koutek, B., Doubsky, J. and Heintz, A.: Vapor pressures and enthalpies of vaporization of a series of the linear aliphatic aldehydes, Fluid Phase Equilibria, 206, 331–339, 2003.

Vesala, T., Kulmala, M., Rudolf, R., Vrtala, A., and Wagner, P. E.: Models for condensational growth and evaporation of binary aerosol particles, J. Aerosol Sci., 28, 565–598, 1997.

Vesna, O., Sax, M., Kalberer, M., Gaschen, A., and Ammann, M.: Product study of oleic acid ozonolysis as function of humidity, Atmos. Environ., 43, 3662–3669, doi:10.1016/j.atmosenv.2009.04.047, 2009.

Vieceli, J., Roeselova, M., Potter, N., Dang, L. X., Garrett, B. C., and Tobias, D. J.: Molecular dynamics simulations of atmospheric oxidants at the air-water interface: Solvation and accommodation of OH and O_3, J. Phys. Chem. B, 109, 15876–15892, doi:10.1021/jp051361+, 2005.

Virtanen, A., Joutsensaari, J., Koop, T., Kannosto, J., YliPirilä, P., J., L., Mäkelä, J. M., Holopainen, J. K., Pöschl, U., Kulmala, M., Worsnop, D. R., and Laaksonen, A.: An amorphous solid state of biogenic secondary organic aerosol particles, Nature, 467, 824–827, doi:10.1038/nature09455, 2010.

Wang, B. and Knopf, D. A.: Heterogeneous ice nucleation on particles composed of humic-like substances impacted by O_3, J. Geophys. Res.-Atmos., 116, D03205, doi:10.1029/2010jd014964, 2011.

Winkler, P. M., Vrtala, A., Wagner, P. E., Kulmala, M., Lehtinen, K. E. J., and Vesala, T.: Mass and thermal accommodation during gas-liquid condensation of water, Phys. Rev. Lett., 93, doi:10.1103/PhysRevLett.93.075701, 2004.article number?

Winkler, P. M., Vrtala, A., Rudolf, R., Wagner, P. E., Riipinen, I., Vesala, T., Lehtinen, K. E. J., Viisanen, Y., and Kulmala, M.: Condensation of water vapor: Experimental determination of mass and thermal accommodation coefficients, J. Geophys. Res.-Atmos., 111, D19202, doi:10.1029/2006jd007194, 2006.

Worsnop, D. R., Morris, J. W., Shi, Q., Davidovits, P., and Kolb, C. E.: A chemical kinetic model for reactive transformations of aerosol particles, Geophys. Res. Lett., 29, 57-1–57-4, doi:10.1029/2002gl015542, 2002.

Xiao, S. and Bertram, A. K.: Reactive uptake kinetics of NO_3 on multicomponent and multi-

phase organic mixtures containing unsaturated and saturated organics, Phys. Chem. Chem. Phys., 13, 6628–6636, doi:10.1039/c0cp02682d, 2011.
Zahardis, J. and Petrucci, G. A.: The oleic acid-ozone heterogeneous reaction system: products, kinetics, secondary chemistry, and atmospheric implications of a model system – a review, Atmos. Chem. Phys., 7, 1237–1274, doi:10.5194/acp-7-1237-2007, 2007.
Ziemann, P. J.: Aerosol products, mechanisms, and kinetics of heterogeneous reactions of ozone with oleic acid in pure and mixed particles, Faraday Discuss., 130, 469–490, doi:10.1039/b417502f, 2005.
Zobrist, B., Marcolli, C., Pedernera, D. A., and Koop, T.: Do atmospheric aerosols form glasses?, Atmos. Chem. Phys., 8, 5221–5244, doi:10.5194/acp-8-5221-2008, 2008.
Zobrist, B., Soonsin, V., Luo, B. P., Krieger, U. K., Marcolli, C., Peter, T., and Koop, T.: Ultra-slow water diffusion in aqueous sucrose glasses, Phys. Chem. Chem. Phys., 13, 3514–3526, doi:10.1039/c0cp01273d, 2011.
Zuend, A., Marcolli, C., Peter, T., and Seinfeld, J. H.: Computation of liquid-liquid equilibria and phase stabilities: implications for RH-dependent gas/particle partitioning of organic-inorganic aerosols, Atmos. Chem. Phys., 10, 7795–7820, doi:10.5194/acp-10-7795-2010, 2010.

Table 1. Thermodynamic and kinetic parameters of air and water used for the simulation of water condensation and droplet growth.

Parameter	Description	Value
$c_{p,a}$	specific heat capacity of dry air at constant pressure (J g^{-1} K^{-1})	1.005[a]
$c_{p,w}$	specific heat capacity of water vapor at constant pressure (J g^{-1} K^{-1})	1.860[a]
$D_{g,w}$	gas diffusion coefficient of water vapor (Torr cm^2 s^{-1})	163[b]
$D_{b,w}$	bulk diffusion coefficient of water (cm^2 s^{-1})	2×10^{-6}
K	thermal conductivity of binary mixtures of air and water vapor (cm^2 s^{-1})	$K_w/(1+0.556p_a/p_w)+K_a/(1+1.189p_w/p_a)$[a]
K_a	thermal conductivity of dry air (J s^{-1} g^{-1} K^{-1})	$3.44 \times 10^{-3} - 7.51 \times 10^{-5}T$[a]
K_v	thermal conductivity of water vapor (J s^{-1} g^{-1} K^{-1})	$-6.72 \times 10^{-3} - 7.49 \times 10^{-5}T^a$
L_w	latent heat of water vaporization (J g^{-1})	$3.14 \times 10^3 - 2.36 \times T$[a]
M_a	molar mass of air (g mol^{-1})	29
M_w	molar mass of water (g mol^{-1})	18
R	gas constant (J K^{-1} mol^{-1})	8.31
ρ_w	density of water (g cm^{-3})	$1.049–1.76 \times 10^{-4} \times T$[a]
$\alpha_{s,0,w}$	surface accommodation coefficient of water on free substrate	0.1–1
α_T	thermal accommodation coefficient of water	1[a]
Σ	surface tension of water (J m^{-2})	$0.0761–1.55 \times 10^{-4}$ $(T-273)$[a]
$\sigma_{s,w}$	effective molecular cross section of H_2O (cm^2)	1.6×10^{-15}
$\tau_{d,w}$	desorption lifetime of H_2O (s)	4×10^{-11}

[a] Winkler et al. (2006), [b] Ivanov et al. (2007)

Table 2. Physical and chemical parameters for oleic acid ozonolysis including the assumed mole-based product yields (compare Zahardis and Petrucci, 2007; all minor products are represented by a dimer with the properties given below).

Parameter	ozone	oleic acid	nonanal	oxononanoic acid	nonanoic acid	azelaic acid	dimer
Yield	–	–	0.6	0.4	0.1	0.1	0.2
$\alpha_{s,0}$	4.2×10^{-4}	–	10^{-2}	–	–	–	–
$\tau_{d,w}$ [s]	0.01	–	10^{-4}	–	–	–	–
ρ [g cm^{-3}]	1.35	0.895	0.827	1.018	0.9	1.225	1.06
$D_{b,Z}$ [cm^2 s^{-1}]	10^{-5}	1.88×10^{-7}	10^{-6}	10^{-6*}	9.17×10^{-7}	10^{-6*}	10^{-10*}
$M_{x,Z}$ [g mol^{-1}]	48	282.46	142.24	172.2	158.23	172.2	622.4

* assumed

Table A1. List of symbols.

Symbol	Description	Unit
α_{b,Z_i}	bulk accommodation coefficient of Z_i	
α_{s,Z_i}	surface accommodation coefficient of Z_i	
α_{ss,Z_i}	quasi-static surface accommodation coefficient of Z_i	
$\alpha_{s,0,Z_i}$	surface accommodation coefficient of Z_i on an adsorbate-free surface	
β_T	transitional correction factor for heat transfer	
$\delta(k)$	thickness of bulk layer k	cm
δ_{Z_i}	effective molecular diameter of Z_i	cm
λ_{Z_i}	mean free path of Z_i in the gas phase	cm
θ_s	sorption layer surface coverage	
θ_{ss}	quasi-static layer surface coverage	
σ_{s,Z_i}	effective molecular cross section of Z_i	cm^2
γ_{Z_i}	uptake coefficient of Z_i	
τ_{d,Z_i}	desorption lifetime of Z_i	s
ω_{Z_i}	mean thermal velocity of Z_i in the gas phase	cm s^{-1}
$A(k)$	outer surface area of bulk layer k	cm^2
A_{ss}	surface area of particle (quasi-static layer)	cm^2
C_{g,Z_i}	gas phase diffusion correction factor for Z_i	
D_{b,Z_i}	bulk diffusion coefficient of Z_i	cm^2 s^{-1}
d_d	particle dry diameter	cm
d_p	particle diameter	cm
H_a	specific enthalpy of dry air	J g^{-1}
H_v	specific enthalpy of moist air	J g^{-1}
H_w	specific enthalpy of water vapor	J g^{-1}
Kn	Knudsen number	
J_{ads,Z_i}	flux of adsorption and desorption of Z_i	cm^{-2} s^{-1}
J_{coll,Z_i}	flux of surface collisions of Z_i	cm^{-2} s^{-1}
J_{b,ss,Z_i}	flux of bulk-to-surface transport of Z_i	cm^{-2} s^{-1}
J_{b1,ss,Z_i}	flux of bulk layer 1-to-surface transport of Z_i	cm^{-2} s^{-1}
J_{s,ss,Z_i}	flux of sorption-to-quasi-static surface layer transport of Z_i	cm^{-2} s^{-1}
J_{ss,s,Z_i}	flux of quasi-static surface-to- sorption layer transport of Z_i	cm^{-2} s^{-1}
J_{ss,b,Z_i}	flux of surface-to-bulk transport of Z_i	cm^{-2} s^{-1}
$J_{ss,b1,Z_i}$	flux of surface-to-bulk layer 1 transport of Z_i	cm^{-2} s^{-1}
k_{a,Z_i}	first-order adsorption rate coefficient of Z_i	
k_{b,ss,Z_i}	rate coefficient (velocity) of bulk-to-surface transport of Z_i	cm s^{-1}

Table A1. List of symbols.

Symbol	Description	Unit
k_{b1,ss,Z_i}	rate coefficient (velocity) of bulk layer 1-to-surface transport of Z_i	cm s^{-1}
k_{BR,Z_p,Z_q}	second-order rate coefficients for bulk reactions of Z_p with Z_q	cm^3 s^{-1}
k_{b,ss,Z_i}	rate coefficient (velocity) of bulk-to-surface transport of Z_j	cm s^{-1}
k_{b1,ss,Z_i}	rate coefficient (velocity) of bulk layer 1-to-surface transport of Z_j	cm s^{-1}
k_{d,Z_i}	first-order desorption rate coefficient of Z_i	s^{-1}
k_{s,ss,Z_i}	first-order rate coefficient for sorption-to-quasi-static surface transport of Z_i	s^{-1}
$k_{ss,b1,Z_i}$	rate coefficient (velocity) of surface-to- bulk layer 1 transport of Z_i	s^{-1}
k_{ss,s,Z_i}	first-order rate coefficients for quasi-static to sorption layer transport of Z_i	s^{-1}
k_{SLR,Z_p,Z_q}	second-order rate coefficients for surface layer reactions of Z_p with Z_q	cm^2 s^{-1}
K_{sol,cc,Z_i}	gas-particle partitioning coefficient of Z_i	
$N_{Z_i,s}$	absolute number of Z_i at surface	
$N_{Z_i,ss}$	absolute number of Z_i at quasi-static surface layer	
$N_{Z_i,bk}$	absolute number of Z_i at bulk layer k	
P_{bk,Z_i}, L_{bk,Z_i}	production (loss) rate of Z_i by reaction in bulk layer k	cm^{-3} s^{-1}
P_{s,Z_i}, L_{s,Z_i}	production (loss) rate of Z_i by sorption surface layer reaction	cm^{-2} s^{-1}
P_{s,ss,Z_i}, L_{s,ss,Z_i}	production (loss) rate of Z_i by sorption – quasi-static surface layer reaction	cm^{-2} s^{-1}
P_{ss,Z_i}, L_{ss,Z_i}	production (loss) rate of Z_i by quasi-static surface layer reaction	cm^{-2} s^{-1}
$r(k)$	radial distance from particle core to bulk layer k	cm
r_p	particle radius	cm
$[Z_i]_g$	gas phase number concentration of Z_i	cm^{-3}
$[Z_i]_{gs}$	near-surface gas phase number concentration of Z_i	cm^{-3}
$[Z_i]_s$	surface number concentration of Z_i (sorption layer)	cm^{-2}
$[Z_i]_{ss}$	surface number concentration of Z_i (quasi-static surface layer)	cm^{-2}
$[Z_i]_{bk}$	bulk number concentration of Z_i in the bulk layer k	cm^{-3}
V_b	volume of particle bulk	cm^{-3}
$V(k)$	volume of bulk layer k	cm^{-3}
V_{Z_i}	molecular volume of Z_i	cm^{-3}

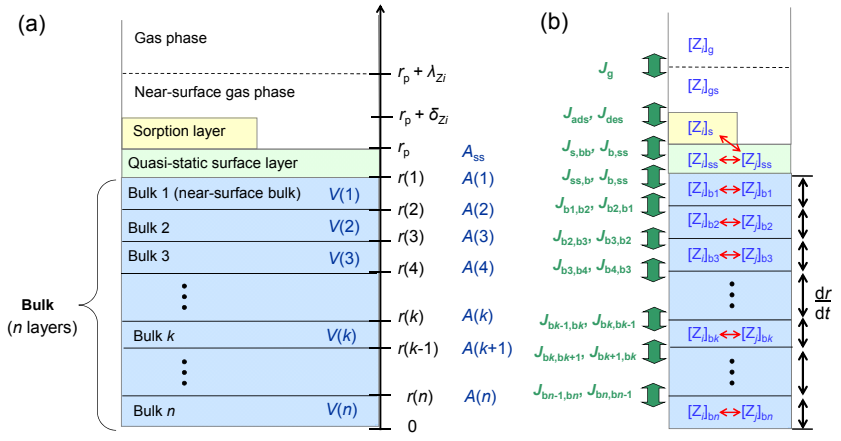

Fig. 1. Kinetic multi-layer model of gas-particle interactions in aerosols and clouds (KM-GAP): **(a)** model compartments and layers with corresponding distances from particle center (r), surface areas (A), and volumes (V). λ_{Z_i} is the mean free path of semi-volatile species Z_i in the gas phase; δ_{Z_i} is the thicknesses of sorption layers. **(b)** Transport fluxes (green arrows) and chemical reactions (red arrows). The black arrows indicate that each bulk layer can grow or shrink.

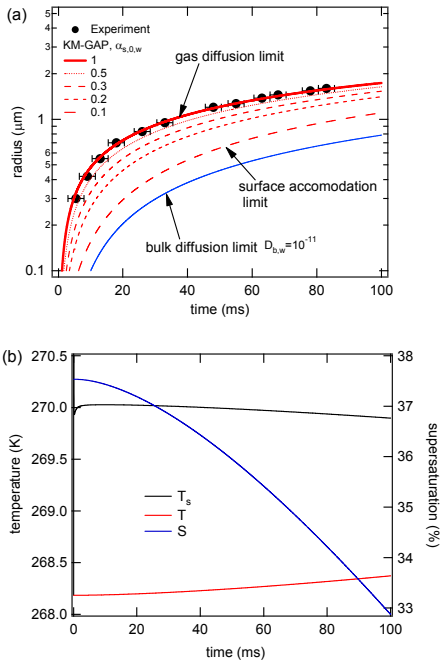

Fig. 2. Water vapor condensation simulated by KM-GAP. **(a)** Water droplet growth curve with different surface accommodation coefficient of H_2O ($\alpha_{s,0,w}$) in comparison with the experimental data by Winkler et al. (2006). The blue line is modeled with low bulk diffusion coefficient ($D_{b,w}$ = 10^{-11} cm^2 s^{-1}) and $\alpha_{s,0,w} = 1$. **(b)** Temporal evolution of surface temperature (T_s, black) and ambient temperature (T, red) and supersaturation (S, blue).

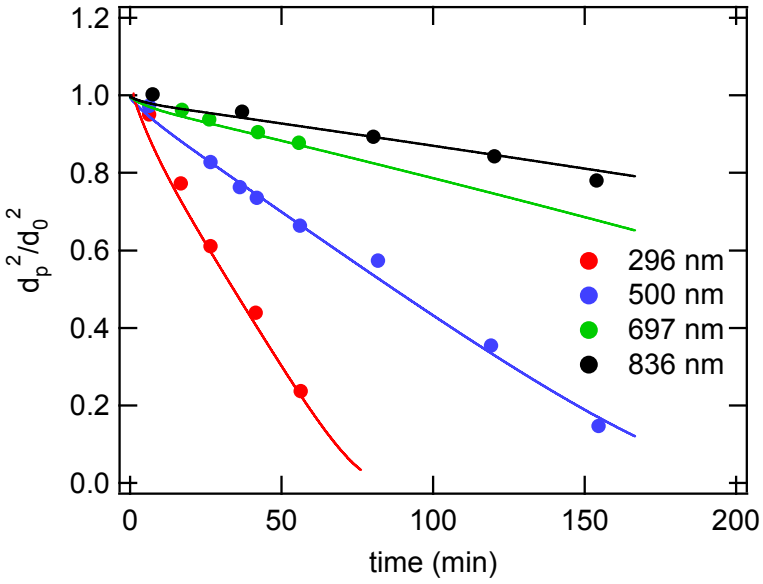

Fig. 3. Evaporation of dioctyl phthalate simulated by KM-GAP as a function of time with particle diameter of 296, 500, 697, and 836 nm. The data points are from Vaden et al. (2011).

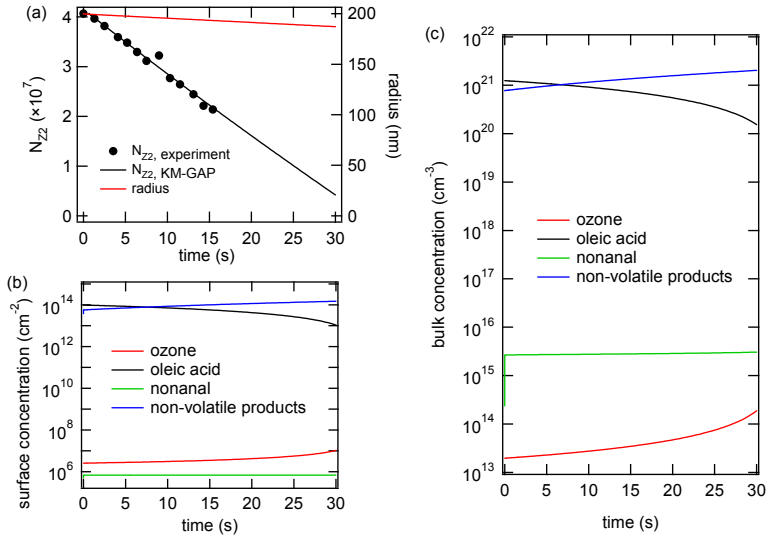

Fig. 4. Ozonolysis of oleic acid and evaporation of nonanal. **(a)** Experimental data (black symbols; Ziemann, 2005) and model results for the total number of oleic acid molecules (N_{Z_2}, black line) and for the particle radius (red line); **(b)** surface concentrations at the quasi-static surface layer and **(c)** average bulk concentration of ozone (red), oleic acid (black), nonanal (green), and non-volatile products (blue).

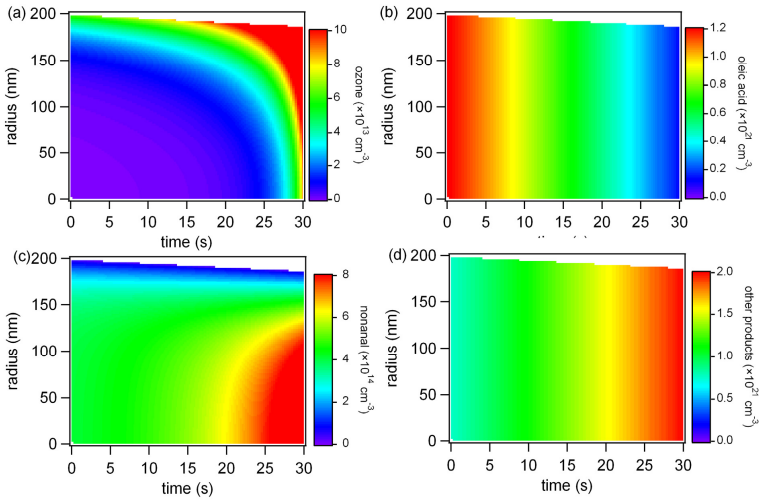

Fig. 5. Ozonolysis of oleic acid and evaporation of nonanal. Temporal evolution of bulk concentration profiles for **(a)** ozone, **(b)** oleic acid, **(b)** nonanal, and **(d)** non-volatile products. The y-axis indicates the radial distance from the particle core to the near-surface bulk. The color shows the bulk concentration in units of cm^{-3} (blue = low, red = high).